

Article

Not peer-reviewed version

---

# Synthesis, Metal-Exchange, and Hyaluronate Functionalization of a Cationic Gallium-Based Thiosemicarbazone Anticancer Drug

---

Ye Ning , Meng-Lin Dong , [Wen-Hua Zhang](#) <sup>\*</sup> , [David James Young](#)

Posted Date: 14 December 2025

doi: [10.20944/preprints202512.1051.v1](https://doi.org/10.20944/preprints202512.1051.v1)

Keywords: gallium-based drugs; thiosemicarbazone; anticancer drugs; drug delivery; metal-exchange



Preprints.org is a free multidisciplinary platform providing preprint service that is dedicated to making early versions of research outputs permanently available and citable. Preprints posted at Preprints.org appear in Web of Science, Crossref, Google Scholar, Scilit, Europe PMC.

Copyright: This open access article is published under a [Creative Commons CC BY 4.0 license](#), which permit the free download, distribution, and reuse, provided that the author and preprint are cited in any reuse.

Disclaimer/Publisher's Note: The statements, opinions, and data contained in all publications are solely those of the individual author(s) and contributor(s) and not of MDPI and/or the editor(s). MDPI and/or the editor(s) disclaim responsibility for any injury to people or property resulting from any ideas, methods, instructions, or products referred to in the content.

## Article

# Synthesis, Metal-Exchange, and Hyaluronate Functionalization of a Cationic Gallium-Based Thiosemicarbazone Anticancer Drug

Ye Ning <sup>1</sup>, Meng-Lin Dong <sup>1</sup>, Wen-Hua Zhang <sup>1,\*</sup> and David J. Young <sup>2</sup>

<sup>1</sup> College of Chemistry, Chemical Engineering, and Materials Science, Soochow University, Suzhou 215123, China

<sup>2</sup> James Watt School of Engineering, Glasgow University, University Avenue, Glasgow, G12 8QQ, UK

\* Correspondence: whzhang@suda.edu.cn

## Abstract

We herein demonstrate that the thiosemicarbazone (TSC) ligand N'-(di(pyridin-2-yl)methylene)-4-(thiazol-2-yl)piperazine-1-carbothiohydrazide (HL) can coordinate with  $\text{Ga}^{3+}$  to give the cationic complex of  $[\text{Ga}(\text{L})_2]\text{NO}_3$  featuring an octahedral  $\text{Ga}(\text{III})$  center.  $[\text{Ga}(\text{L})_2]\text{NO}_3$  may undergo metathesis with both  $\text{Fe}^{2+}$  and  $\text{Fe}^{3+}$  and result in the formation of respective  $\text{Fe}^{2+}$ - and  $\text{Fe}^{3+}$  complex. Meanwhile,  $[\text{Ga}(\text{L})_2]\text{NO}_3$  is also susceptible to anion exchange with solidum hyaluronate ( $\text{NaA}$ ) to produce the nanoformulation of  $[\text{Ga}(\text{L})_2]\text{A}$  with boosted aqueous solubility and cell targetability.  $[\text{Ga}(\text{L})_2]\text{A}$  demonstrated remarkable *in vitro* cytotoxicity against NCI-H82 and A549 (lung cancer), as well as KYSE-510 and Te-1 (esophageal cancer) cell lines, featuring half maximal inhibitory concentration ( $\text{IC}_{50}$ ) values in the range of  $0.102 - 2.616 \mu\text{mol L}^{-1}$ . This work highlights the potential of using non-toxic and biocompatible  $\text{Ga}^{3+}$  as the central ion to prepare TSC-based nanomedicines for combating cancer.

**Keywords:** gallium-based drugs; thiosemicarbazone; anticancer drugs; drug delivery; metal-exchange

## 1. Introduction

Thiosemicarbazones (TSCs) are a class of Schiff-base derivatives that have been widely documented as a type of highly promising anticancer drugs for a broad-spectrum of cancer types through diverse mechanisms [1-4]. As a type of N- and S- rich metal chelators, TSCs can elicit their anticancer effect via quick sequestration of cell-proliferative-dependent ions of  $\text{Fe}^{3+}$  [4]. On the other hand, the anticancer effect of TSCs is profoundly affected by their structures [2,4-6]. In particular, placement of an additional N coordination site, such as  $\alpha$ -pyridyl, serves as an advantage as it forms a more stable N, N, S tridentate chelation that results in more effective ion removal [7-9]. The promising anticancer potential of TSCs has been showcased by several drugs that successfully entered clinical trials, such as Triapine, 5-HP, and COTI-2 [10-13].

Gallium (Ga), though with limited physiological function in the human body, demonstrated important biological properties [14,15]. For example,  $\text{Ga}^{3+}$  is effective in suppressing bone resorption and simultaneously elevating plasma calcium [15]. It is used in the clinics for the treatment of hypercalcemia of malignancy and Paget's disease of bone [16].  $\text{Ga}^{3+}$  has also shown clinical efficacy in suppressing osteolysis and bone pain associated with multiple myeloma and bone metastases, and has been suggested as a treatment for osteoporosis [14].

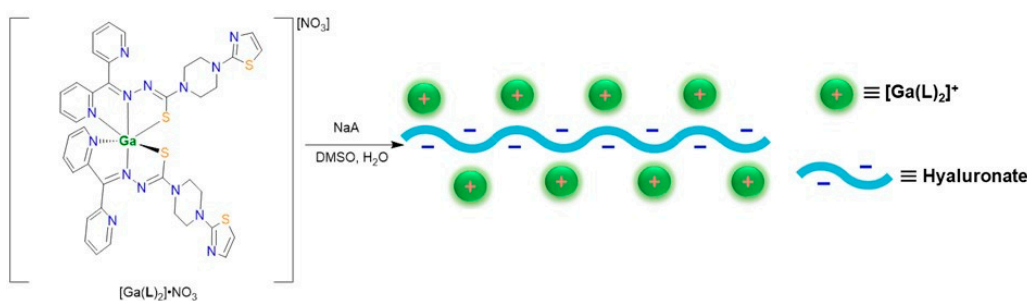
It is notable that  $\text{Ga}^{3+}$  and  $\text{Fe}^{3+}$  share a very similar charge-to-radius ratio, and the chemical behavior of  $\text{Ga}^{3+}$  closely resembles that of  $\text{Fe}^{3+}$  [15,17,18]. Due to this reason,  $\text{Ga}^{3+}$  can bind to the iron-transport protein transferrin (Tf), although the affinity of Tf for  $\text{Fe}^{3+}$  is much higher than that for  $\text{Ga}^{3+}$ ,

and the replacement of  $\text{Ga}^{3+}$  by  $\text{Fe}^{3+}$  occurs very slowly [15]. In comparison,  $\text{Ga}^{3+}$  is unable to enter  $\text{Fe}^{2+}$ -containing proteins, such as hemoglobin and cytochromes. Hence, it does not enter red blood cells and does not interfere with oxygen transport [15].

Intrigued by the profound link between  $\text{Ga}^{3+}$  and  $\text{Fe}^{3+}$ , an ion that is critical to the rigorous metabolism of cancer cells,  $\text{Ga}(\text{III})$ -based drugs have been widely developed to target the  $\text{Fe}^{3+}$ -dependent metabolism [6,19-21]. For example, tris(8-quinolinolato)-gallium(III) (KP46), originally evaluated to show better bioavailability and higher toxicity than  $\text{GaCl}_3$  upon oral administration, are enjoying a continuous interest in treating various cancers, such as melanoma and renal cell carcinoma [19]. KP46 is also found to sensitize resistant leukemia cells and overcome  $\text{Bcl-2}$ -induced multidrug resistance in lymphoma cells via upregulation of Harakiri and downregulation of XIAP in vitro [20].  $\text{Ga}(\text{III})$  complexes with cloxyquin ligands are also reported to induce ferroptosis in cancer cells [21]. Using human cancer cell lines 41M and SK-BR-3 as models, Arion and Keppler et al revealed that the coordination of  $\text{Ga}^{3+}$  to TSCs unequivocally and specifically modulates the cytotoxic potency in a beneficial manner, whereas surrogation of  $\text{Ga}^{3+}$  with  $\text{Fe}^{3+}$  impairs the biological activity [6].

In our recent work, we reported the synthesis of a new TSC-based anticancer drug of  $\text{N}'$ -(di(pyridin-2-yl)methylene)-4-(thiazol-2-yl)piperazine-1-carbothiohydrazide (HL) featuring di-2-pyridylketone moiety with chelating-bridging functions [22]. Ligand HL can readily associate with  $\text{Cu}^{2+}$  to give the corresponding coordination complexes that demonstrated superior anticancer performances against hepatocellular carcinoma, which involved reactive oxygen species generation. Pharmacokinetic studies also revealed that HL can be successfully absorbed via oral administration, with a favorable half-life that is nearly double that of intravenous administration, rendering HL a clinically promising oral drug.

Herein, we explore the reaction of HL with  $\text{Ga}(\text{NO}_3)_3 \cdot 9\text{H}_2\text{O}$  and obtain the anticipated octahedral complex of  $[\text{Ga}(\text{L})_2]\text{NO}_3$  (Scheme 1 and Figure 1a).  $[\text{Ga}(\text{L})_2]\text{NO}_3$  may undergo metathesis with both  $\text{Fe}^{2+}$  and  $\text{Fe}^{3+}$  to yield the respective  $\text{Fe}^{2+}$ - and  $\text{Fe}^{3+}$ -based complexes quantitatively. The ionic nature of  $[\text{Ga}(\text{L})_2]\text{NO}_3$  further permits its anion exchange reaction with sodium hyaluronate ( $\text{NaA}$ ) to give the corresponding nanoformulation of  $[\text{Ga}(\text{L})_2]\text{A}$  to endow the material with aqueous solubility and targetability (Scheme 1) [23-25]. Our preliminary results suggest that  $[\text{Ga}(\text{L})_2]\text{A}$  exhibits pronounced cytotoxicity in cell lines NCI-H82 and A549 (lung cancer), as well as KYSE-510 and Te-1 (esophageal cancer). This work highlights the promising potential of anticancer nanomedicines from non-toxic and biocompatible  $\text{Ga}^{3+}$  and TSC ligands.



**Scheme 1.** Synthesis of  $[\text{Ga}(\text{L})_2]\text{NO}_3$  and its anion exchange with  $\text{NaA}$  to give  $[\text{Ga}(\text{L})_2]\text{A}$ .

## 2. Results and Discussion

### 2.1. Synthesis and Structure of $[\text{Ga}(\text{L})_2]\text{NO}_3$

The ligand HL was synthesized according to our previously reported procedures [22]. HL and similar ligand types featuring  $\text{N},\text{N},\text{S}$ -chelation functions are demonstrated to associate with diverse metal ions, dominantly those biologically relevant  $\text{Fe}^{2+}/\text{Fe}^{3+}$  [6,26,27],  $\text{Cu}^{+2}/\text{Cu}^{2+}$  [28-30], and  $\text{Zn}^{2+}$  [31,32], due to their soft-hard hybrid combinations. Herein, the reaction of  $\text{Ga}(\text{NO}_3)_3 \cdot 9\text{H}_2\text{O}$  and HL in MeOH at ambient conditions, followed by ether diffusion, gives rise to  $[\text{Ga}(\text{L})_2]\text{NO}_3$  as yellow block crystals in

23.3% yield. Crystal of  $[\text{Ga}(\text{L})_2]\text{NO}_3$  is soluble in common solvents ranging from polar to medium polar solvents, such as  $\text{H}_2\text{O}$ ,  $\text{MeOH}$ ,  $\text{DMSO}$ ,  $\text{DMF}$ , and  $\text{CH}_2\text{Cl}_2$ .

Compound  $[\text{Ga}(\text{L})_2]\text{NO}_3$  crystallizes in the monoclinic space group  $P2_1/n$  (Table 1), and its asymmetric unit contains a full  $[\text{Ga}(\text{L})_2]\text{NO}_3$  molecule along with a  $\text{MeOH}$  solvate (Figure 1b). The octahedral coordination preference of  $\text{Ga}^{3+}$  enables the chelation of a pair of ligands to give the  $[\text{Ga}(\text{L})_2]^+$  cation, which is accompanied by an  $\text{NO}_3^-$  counterion. This further indicates that the ligand is tautomerized toward its enol form (thiol), which is subsequently deprotonated [33,34].

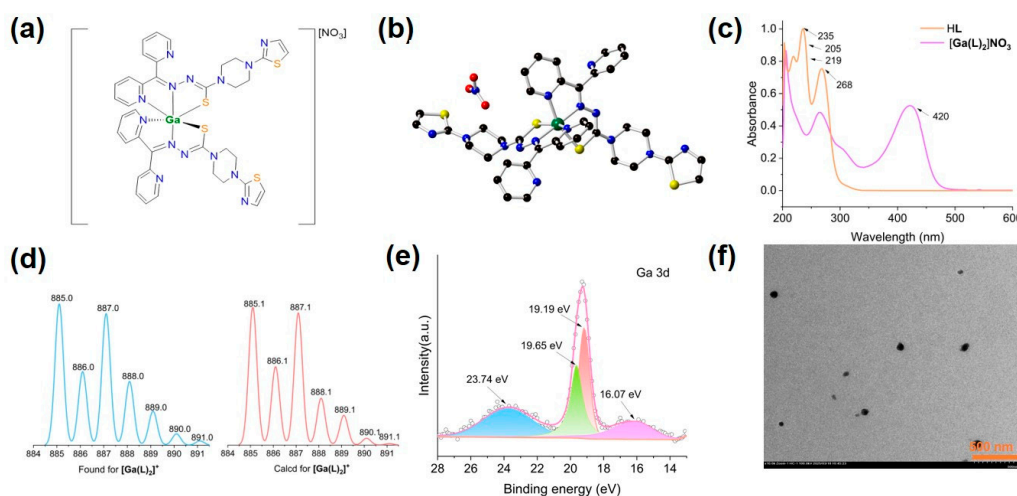


**Figure 1.** The chemical diagram (a) and crystal structure (b) of  $[\text{Ga}(\text{L})_2]\text{NO}_3$ . The UV-Vis spectra of HL and  $[\text{Ga}(\text{L})_2]\text{NO}_3$  in  $\text{CH}_2\text{Cl}_2$  solution (c). The HPLC-MS results of  $[\text{Ga}(\text{L})_2]\text{NO}_3$ , as demonstrated by the consistency between the experimental (blue) and calculated (orange) peak values and patterns (d) assignable as  $[\text{Ga}(\text{L})_2]^+$ . The Ga 3d XPS spectra of  $[\text{Ga}(\text{L})_2]\text{NO}_3$  (e), and the TEM image of  $[\text{Ga}(\text{L})_2]\text{A}$  (f). For (b), the  $\text{MeOH}$  solvate and hydrogen atoms are omitted for clarity. Color legend: Ga (dark green), S (yellow), O (red), N (blue), and C (black).

**Table 1.** Crystal data and structure refinement parameters for  $[\text{Ga}(\text{L})_2]\text{NO}_3$ .

|   | $[\text{Ga}(\text{L})_2]\text{NO}_3$                            |
|---|---|
| Formula                                 | $\text{C}_{39}\text{H}_{40}\text{GaN}_{15}\text{O}_4\text{S}_4$ |
| Formula Weight                          | 980.82  |
| Crystal System                          | monoclinic  |
| Space Group                             | $P2_1/n$  |
| $a/\text{\AA}$                          | 13.7231(4)  |
| $b/\text{\AA}$                          | 16.5511(5)  |
| $c/\text{\AA}$                          | 19.3202(7)  |
| $\beta/^\circ$                          | 93.1060(10)   |
| $V/\text{\AA}^3$                        | 4381.8(2)   |
| $Z$                                     | 4   |
| $\rho_{\text{calc}}/(\text{g cm}^{-3})$ | 1.487   |
| $F(000)$                                | 2024  |
| $\mu(\text{Mo-K}\alpha)/\text{mm}^{-1}$ | 0.879   |
| Total Reflections                       | 102760  |
| Unique Reflections                      | 10031   |
| No. Observations                        | 8243  |
| $R_{\text{int}}$                        | 0.0528  |
| No. Parameters                          | 570   |
| $R^a$                                   | 0.0374  |
| $wR^b$                                  | 0.0912  |
| $GOF^c$                                 | 1.111   |

<sup>a</sup>  $R_1 = \Sigma ||F_o| - |F_c|| / \Sigma |F_o|$ , <sup>b</sup>  $wR_2 = \{\Sigma [w(F_o^2 - F_c^2)^2] / \Sigma [w(F_o^2)^2]\}^{1/2}$ , <sup>c</sup> GOF =  $\{\Sigma [w(F_o^2 - F_c^2)^2] / (n-p)\}^{1/2}$ , where  $n$  is the number of reflections and  $p$  is total number of parameters refined.

In  $[\text{Ga}(\text{L})_2]\text{NO}_3$ , the Ga–S bond distances (2.3600(6) and 2.3715(6) Å, Table 2) are similar to those reported in the literature, such as those in [bis(acetylpyrazine N,N-dimethylthiosemicarbazone)-N,N,S-gallium(III)] hexafluorophosphate (2.3321(7) and 2.3532(9) Å) [6], and [bis(acetylpyrazine N-pyrrolidinylthiosemicarbazone)-N,N,S-gallium(III)] hexafluorophosphate (2.3389(6) and 2.3525(6) Å) [6]. It should be noted that, though  $\text{Ga}^{3+}$  and  $\text{Fe}^{3+}$  share a similar ionic radius, their respective  $\text{Fe}^{3+}$ -based complexes using the same TSC ligand exhibit marginally shorter Fe–S bond distances. For example, the Fe–S bond distances in [bis(acetylpyrazine N,N-dimethylthiosemicarbazone)-N,N,S-iron(III)] tetrachloroferrate(III) are 2.2242(6) and 2.2341(7) Å [6], similar to those found in [bis(acetylpyrazine N-pyrrolidinylthiosemicarbazone)-N,N,S-iron(III)] tetrachloroferrate(III) (2.2156(9) and 2.2322(10) Å) [6]. A similar trend is also observed in other Fe-TSC complexes, such as the  $\text{Fe}^{3+}$  complex of 4-(4-Nitrophenyl)-1-((pyridin-2-yl)methylene)thiosemicbazide (2.2161(6) and 2.2009(9) Å) [35]. The shorter Fe–S bond distances as compared to those of Ga–S probably serve as the driving force for their metathesis reactions to yield the more stable Fe-based species.

**Table 2.** Selected bond distances (Å) and angles (°) of  $[\text{Ga}(\text{L})_2]\text{NO}_3$  involving the Ga(III) center.

| Ga1–S1     | 2.3600(6)  | Ga1–S3      | 2.3715(6)  |
|------------|------------|-------------|------------|
| Ga1–N12    | 2.0493(17) | Ga1–N5      | 2.0529(16) |
| Ga1–N7     | 2.0938(18) | Ga1–N13     | 2.1249(18) |
| N12–Ga1–N5 | 175.06(7)  | N12–Ga1–N7  | 97.70(7)   |
| N5–Ga1–N7  | 78.03(7)   | N12–Ga1–N13 | 77.30(7)   |
| N5–Ga1–N13 | 99.88(7)   | N7–Ga1–N13  | 87.69(7)   |
| N12–Ga1–S1 | 101.96(5)  | N5–Ga1–S1   | 82.07(5)   |
| N7–Ga1–S1  | 159.62(5)  | N13–Ga1–S1  | 91.44(5)   |
| N12–Ga1–S3 | 82.12(5)   | N5–Ga1–S3   | 100.30(5)  |
| N7–Ga1–S3  | 90.52(5)   | N13–Ga1–S3  | 158.91(5)  |
| S1–Ga1–S3  | 97.36(2)   |             |            |

## 2.2. Spectroscopic and Spectrometric Characterizations of $[\text{Ga}(\text{L})_2]\text{NO}_3$

The high-performance liquid chromatography – mass spectrometry (HPLC-MS) revealed signals at 885.0 m/z for  $[\text{Ga}(\text{L})_2]\text{NO}_3$  corresponding to  $[\text{Ga}(\text{L})_2]^+$  (calculated 885.1 m/z) (Figure 1d). The <sup>1</sup>H nuclear magnetic resonance (<sup>1</sup>H NMR) spectra show that the thiosemicarbazone proton peak at 14.64 ppm in HL is absent in  $[\text{Ga}(\text{L})_2]\text{NO}_3$  (Figure S1), providing evidence of the thione-to-thiol tautomerism and subsequent  $\text{Ga}^{3+}$  coordination by eliminating the thiol proton.

The Fourier-transform infrared (FT-IR) spectroscopic analysis revealed significant coordination-induced modifications in the vibrational modes. The  $\nu_{(\text{C}=\text{S})}$  vibration at 869 cm<sup>-1</sup> in the free ligand HL bathochromically shifted to 854 cm<sup>-1</sup> in  $[\text{Ga}(\text{L})_2]\text{NO}_3$  (Figure S2) [36]. In contrast, the C=N stretching vibration of HL, originally observed at 1579 cm<sup>-1</sup> in the FT-IR spectrum, hypsochromically shifted to 1598 cm<sup>-1</sup> upon coordination with  $\text{Ga}^{3+}$  in  $[\text{Ga}(\text{L})_2]\text{NO}_3$  [37–39]. In addition, a sharp peak at 1362 cm<sup>-1</sup>, characteristic for the presence of  $\text{NO}_3^-$  [40], is also identified.

The ultraviolet-visible (UV-Vis) spectral analysis revealed that, in comparison to HL,  $[\text{Ga}(\text{L})_2]\text{NO}_3$  demonstrated distinct absorption bands at 420 nm (Figure 1c), which are characteristic of ligand-to-metal charge transfer (LMCT) transitions [39]. This spectral evidence confirms the successful formation of coordination bonds between the Ga(III) center and the organic ligand.

Energy dispersive X-ray spectroscopy (EDS) revealed an atomic ratio of Ga : S = 0.9 : 4.0 (equivalent to 1.0 : 4.4) for  $[\text{Ga}(\text{L})_2]\text{NO}_3$  (Figure S3), consistent with the derived ratio of Ga : S ratio of 1 : 4 from the single-crystal data. X-ray photoelectron spectroscopy (XPS) of  $[\text{Ga}(\text{L})_2]\text{NO}_3$  confirmed the presence of C, N, O, and  $\text{Ga}^{3+}$  (Figure S4). The Ga 3d XPS of  $[\text{Ga}(\text{L})_2]\text{NO}_3$  showed two peaks at binding energies of 19.19 eV and 19.65 eV, which are assignable to the spin-orbit splitting of Ga 3d<sub>5/2</sub>

and Ga 3d<sub>3/2</sub> of Ga<sup>3+</sup> (Figure 1e) [41-43]. The N, N, S-conjugated tridentate moiety in the thiosemicarbazone ligand exhibits high electron cloud density and strong coordinating capability, potentially leading to a slight decrease in the binding energy of Ga 3d orbitals [41].

### 2.3. Fe<sup>2+</sup> and Fe<sup>3+</sup> Exchange with [Ga(L)<sub>2</sub>]NO<sub>3</sub>

[Ga(L)<sub>2</sub>]NO<sub>3</sub> can smoothly undergo transmetalation with Fe<sup>2+</sup> (using (NH<sub>4</sub>)<sub>2</sub>Fe(SO<sub>4</sub>)<sub>2</sub>·6H<sub>2</sub>O) and Fe<sup>3+</sup> (using NH<sub>4</sub>Fe(SO<sub>4</sub>)<sub>2</sub>·12H<sub>2</sub>O) in DMF. For the transmetalation with Fe<sup>2+</sup>, the solution color gradually changed from light green to dark green (Figure S5), while for that of Fe<sup>3+</sup>, the solution color gradually changed to yellowish-brown (Figure S6), presumably driven by the more stable complex formation. EDS of the exchanged samples indeed indicated that for both reactions, the Ga<sup>3+</sup> is totally removed (Figures S7).

Titration experiment in DMF-H<sub>2</sub>O indicates that for Fe<sup>2+</sup> exchange, the LMCT band at 426 nm gradually shifted to 400 nm (Figure 2a), accompanied by the appearance of a new band at 644 nm, assignable as the lower energy charge transfer transition from the thiolate sulfur to Fe<sup>2+</sup>, which is unique for Fe(II)-TSC complexes [44]. It is interesting to note that, for the metathesis with Fe<sup>3+</sup>, the reaction initially generated Fe<sup>2+</sup> species characterized by the generation of a low-energy peak at 657 nm (Figure 2b), presumably due to the reductive nature of the thiols [24,25]. Meanwhile, the LMCT band of [Ga(L)<sub>2</sub>]NO<sub>3</sub> gradually blue-shifted from 426 nm to 406 nm, accompanied by a shoulder peak at 484 nm, characterized for Fe<sup>3+</sup> bonding [45]. We further observed that the transmetalation reaction proceeds rather smoothly, as indicated by these titration curves and sample photographs recorded 0.5 h, 6 h, and 72 h (Figures S5 and S6).

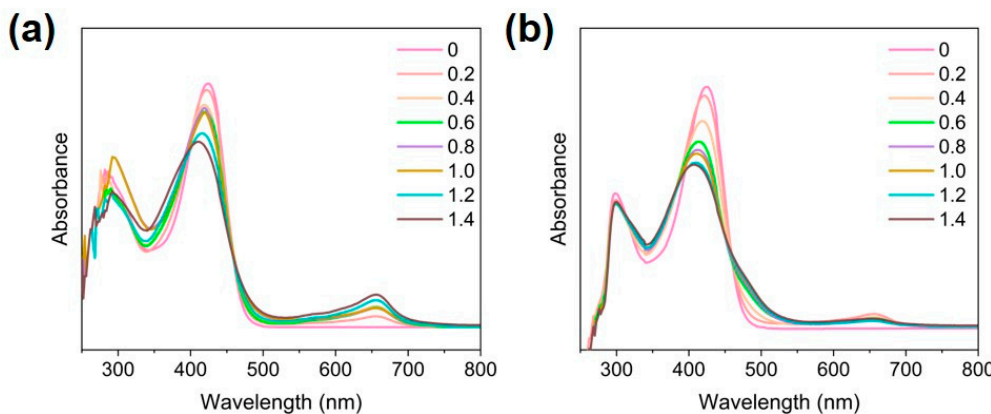


**Figure 2.** UV-Vis spectral changes observed during the titration of [Ga(L)<sub>2</sub>]NO<sub>3</sub> with (NH<sub>4</sub>)<sub>2</sub>Fe(SO<sub>4</sub>)<sub>2</sub>·6H<sub>2</sub>O (a) and with NH<sub>4</sub>Fe(SO<sub>4</sub>)<sub>2</sub>·12H<sub>2</sub>O (b). For each titration, a 1.0 equivalent solution of the Ga(III) complex in DMF was successively titrated with 0.2 equivalent aliquots of the respective iron salt.

### 2.4. Synthesis and Characterizations of [Ga(L)<sub>2</sub>]A Nanoparticles

Hyaluronic acid (HA) has been widely used for the delivery of drug molecules as hyaluronan receptor CD-44 is overexpressed in numerous cancer cell lines [46-48]. Chemically, HA is rich in coordination motifs (i.e. carboxylates and hydroxyls) that can be particularly useful for the delivery of metal-based medicines via binding to the metal ions. Herein, the sodium salt of HA, viz., NaA, serves as an additional advantage to form stable complexes with [Ga(L)<sub>2</sub>]NO<sub>3</sub> via the ejection of NaNO<sub>3</sub>. The [Ga(L)<sub>2</sub>]A nanoparticles were prepared by stirring a DMSO solution of [Ga(L)<sub>2</sub>]NO<sub>3</sub> and an aqueous solution of NaA followed by dialysis using a membrane with a molecular weight cutoff of 1000 Da. FT-IR spectroscopy shows that the peak at 1362 cm<sup>-1</sup> (Figure S2), characteristic for NO<sub>3</sub><sup>-</sup>, is absent in [Ga(L)<sub>2</sub>]A, indicating that the anion exchange process is complete [40].

Transmission electron microscopy (TEM) indicated that the particle sizes for [Ga(L)<sub>2</sub>]A are around 100 nm (Figure 1f), which is conducive to cellular uptake. The average hydrodynamic diameters of these particles, determined by dynamic light scattering (DLS), were measured to be 195.2

nm (PDI = 0.456) (Figure S8). These DLS measurements are significantly larger than the corresponding TEM-derived values due to the hydration of the micelles [25,49]. The zeta potential for  $[\text{Ga}(\text{L}_2)\text{A}]$  is  $-26.1$  mV, which is significantly different from that of  $[\text{Ga}(\text{L}_2)\text{NO}_3]$  (3.09 mV) (Figure S9). Materials with neutral or positive zeta potentials generally exhibit enhanced cell binding affinity with cell membranes, though this may concurrently increase systemic toxicity [50]. Conversely, materials with negative zeta potentials, such as those described herein, are more likely to maintain prolonged plasma circulation, thereby optimizing enhanced cell permeability and retention (EPR) [51,52].

### 2.5. Cell Cytotoxicity Assay

To evaluate the anticancer potency of  $[\text{Ga}(\text{L}_2)\text{A}]$ , we assessed their inhibitory rates against four cancer cell lines: NCI-H82 (lung cancer), A549 (lung cancer), KYSE-510 (esophageal cancer), and Te-1 (esophageal cancer), and compared them with those for HL. As shown in Figures 3a – 3h, both HL and  $[\text{Ga}(\text{L}_2)\text{A}]$  exhibited superior in vitro cytotoxicity against all these cell lines, featuring half maximal inhibitory concentration ( $\text{IC}_{50}$ ) values in the range of  $0.102$  –  $2.616$   $\mu\text{mol L}^{-1}$  (Table 3), and are comparable to those  $\text{Ga}^{3+}$ - and  $\text{Fe}^{3+}$ -based TSC complexes reported in the literature, indicating the potency of  $[\text{Ga}(\text{L}_2)\text{A}]$  in killing diverse cancer cells.

**Table 3.** A comparison of the  $\text{IC}_{50}$  values of HL and  $[\text{Ga}(\text{L}_2)\text{A}]$  with literature examples toward different cell lines.

| Entry | Compound  | Cell Line  | $\text{IC}_{50}$ ( $\mu\text{M}$ ) | Reference |
|-------|---|------------|------------------------------------|-----------|
| 1     | $[\text{Ga}(\text{L}_a)_2\text{NO}_3]$                              | RT2        | 810                                | [53]      |
| 2     | $[\text{Ga}(\text{L}_b)_2(\text{NO}_3)_2]\cdot x\text{H}_2\text{O}$ | HCT-116    | 0.55                               | [54]      |
| 3     | $[\text{Ga}(\text{L}_c)_2]\text{PF}_6$                              | SK-BR-3    | $1.7\times 10^{-4}$                | [6]       |
| 4     | $[\text{Ga}(\text{L}_d)\text{Cl}_2]$                                | MCF-7      | 1.05                               | [55]      |
| 5     | $[\text{Fe}(\text{L}_e)_2](\text{ClO}_4)_2$                         | SK-N-MC    | 0.19                               | [56]      |
| 6     | $[\text{Fe}(\text{L}_f)_2(\text{NO}_3)_2(\text{H}_2\text{O})_3]$    | SW-480     | 19.11                              | [45]      |
| 7     | $[\text{Fe}(\text{L}_g)_2](\text{ClO}_4)_2$                         | HL60       | 0.4                                | [57]      |
| 8     | $[\text{Fe}(\text{L}_h)_2]\text{Cl}$                                | MDA-MB-231 | 12.38                              | [58]      |
| 9     | $[\text{Cu}(\text{NO}_3)_2(\text{L})_2]$                            | Hep-G2     | 16.86                              | [22]      |
| 11    | $[\text{Ga}(\text{L})_2]\text{A}$                                   | NCI-H82    | 0.102                              | This work |
| 12    | $[\text{Ga}(\text{L})_2]\text{A}$                                   | A549       | 1.342                              | This work |
| 13    | $[\text{Ga}(\text{L})_2]\text{A}$                                   | KYSE-510   | 2.616                              | This work |
| 14    | $[\text{Ga}(\text{L})_2]\text{A}$                                   | Te-1       | 0.267                              | This work |

$\text{L}_a$  = N(4)-methyl-2-pyridineformamide thiosemicarbazone;  $\text{L}_b$  =  $\text{N}^1$ -(7-chloro-quinolin-4-yl)-ethylamino-2-acetylpyridine-thiosemicarbazone;  $\text{L}_c$  = acetylpyrazine N,N-dimethylthiosemicarbazone;  $\text{L}_d$  = isopropyl-2-pyridyl-ketone-4,4-dimethylthiosemicarbazone;  $\text{L}_e$  = (Z)-3-phenyl-1-(2-pyridinyl)-2-propen-1-one-4,4-dimethyl-3-thiosemicarbazone;  $\text{L}_f$  = pyridine-2-carbaldehyde 4N-methylthiosemicarbazone;  $\text{L}_g$  = dipyridylketone 4-allylthiosemicarbazone;  $\text{L}_h$  = 2-benzoylpyridine 4-methyl-3-thiosemicarbazone.

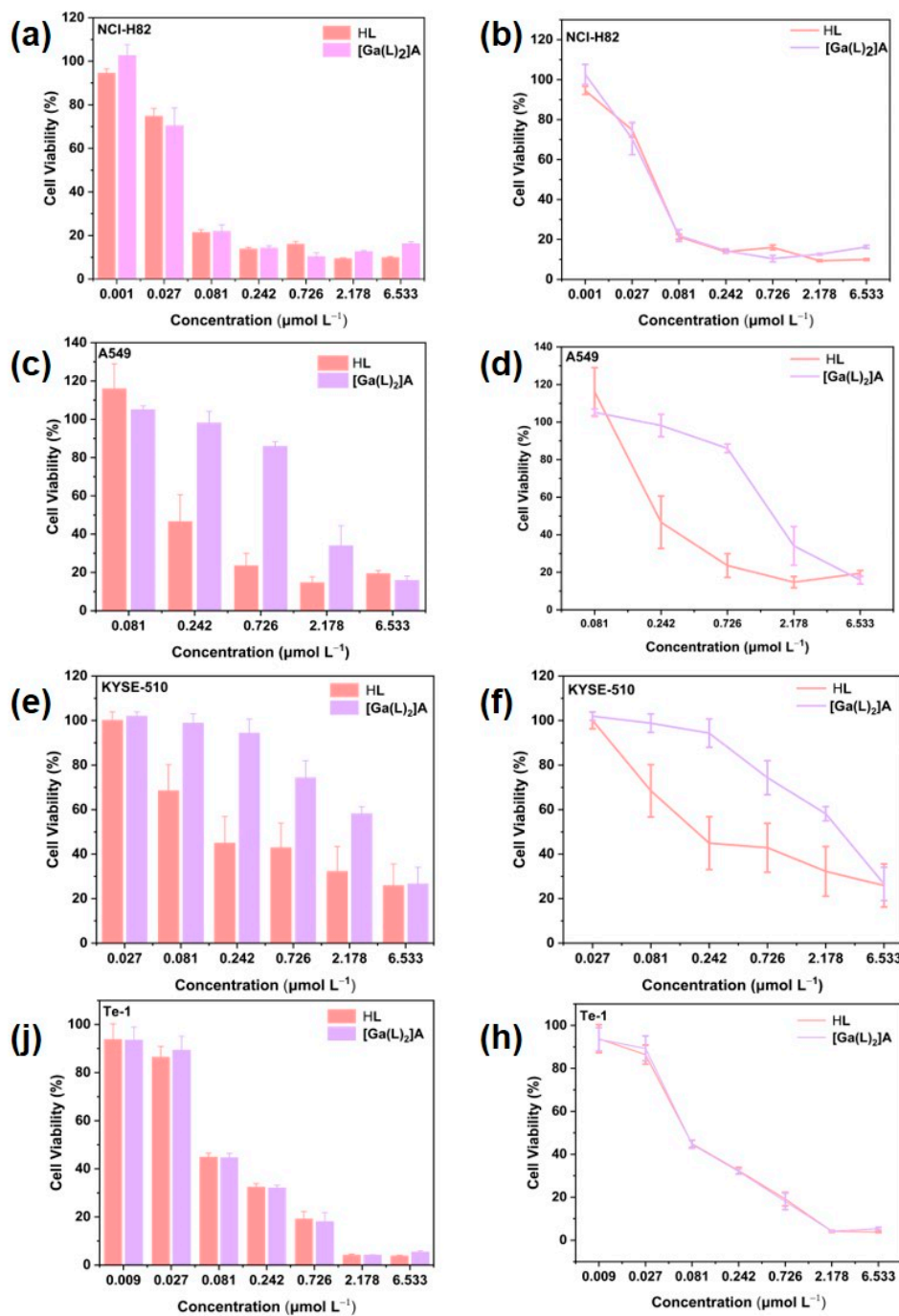


**Figure 3.** A comparison of cell viability of NCI-H82 (a, b), A549 (c, d), KYSE-510 (e, f), and Te-1 (j, h) upon incubation with gradient concentrations HL and  $[\text{Ga}(\text{L})_2]\text{A}$ .

#### 2.6. Cellular Uptake of $[\text{Ga}(\text{L})_2]\text{A}$

To evaluate the contribution of hyaluronate in the cellular uptake process, we pretreated KYSE-510 cells as a representative with NaA followed by a dosage of  $[\text{Ga}(\text{L})_2]\text{A}$  (NaA-pretreated cells are denoted as  $[\text{Ga}(\text{L})_2]\text{A}'$ ), and compared the results with those of directly administered  $[\text{Ga}(\text{L})_2]\text{A}$ . As shown in Table 4, the inductively coupled plasma mass spectrometric data (ICP-MS) show that, regardless of the presence of NaA, the drug uptake by the cells increased with incubation time. However, the uptake of  $[\text{Ga}(\text{L})_2]\text{A}$  by KYSE-510 cells pretreated with NaA was marginally lower than that of cells directly treated with  $[\text{Ga}(\text{L})_2]\text{A}$ . These results indicate that the drug  $[\text{Ga}(\text{L})_2]\text{A}$  modified by hyaluronic acid has a CD-44 targeting effect.

**Table 4.** Cellular uptake of  $[\text{Ga}(\text{L})_2]\text{A}$  by KYSE-510 ( $1 \times 10^7$  cells) with and without NaA pre-treatment, as determined by  $\text{Ga}^{3+}$  concentration (ppb) using ICP-MS. The NaA pre-treated sample is denoted as  $[\text{Ga}(\text{L})_2]\text{A}'$ .

|     | $[\text{Ga}(\text{L})_2]\text{A}$ | $[\text{Ga}(\text{L})_2]\text{A}'$ |
|-----|-----------------------------------|------------------------------------|
| 2 h | 310.325                           | 224.521                            |
| 4 h | 503.897                           | 309.679                            |
| 6 h | 554.22                            | 323.187                            |

### 3. Materials and Methods

#### 3.1. General

Ligand HL was synthesized as described in our previous report [22].  $\text{Ga}(\text{NO}_3)_3 \cdot 9\text{H}_2\text{O}$  (99.99%, Xiya Chemical Technology (Shandong) Co., Ltd) and sodium hyaluronate (97%, Energy Chemicals) were available from the corresponding suppliers without further purification. MeOH, N, N-dimethylformamide (DMF), dimethyl sulfoxide (DMSO), and diethyl ether ( $\text{Et}_2\text{O}$ ), all in analytical grade, were procured from Chinasun Specialty Products Co., Ltd.

Cell lines NCI-H82, A549, KYSE-510, and Te-1 cell lines were purchased from the Shanghai Institute of Cell Biology, Chinese Academy of Sciences. 0.25% trypsin solution (containing EDTA, dissolved in PBS) was purchased from Procell Life Science & Technology Co., Ltd. Cell culturing medium RPMI 1640 (10% FBS + 1% P/S), RPMI 1640 (1% P/S), Ham's F-12 (10% FBS + 1% P/S), Ham's F-12 (1% P/S), and Phosphate buffer solution (PBS) were purchased from Shanghai Basal Media Technologies Co., Ltd. The cell counting kit-8 (CCK-8) was from APEXBIO. The determination of HL concentration in all experiments was based on deionized water using a standard curve (Figure S10).

$^1\text{H}$  nuclear magnetic resonance (NMR) spectra were recorded on a BRUKER AVANCE III HD 400 MHz superconducting NMR spectrometer (Bruker AXS GmbH, Germany). Fourier-transform infrared (FT-IR) spectra were measured using a Bruker VERTEX 70 + HYPERION 2000 FT-IR spectrometer (Bruker AXS GmbH, Germany), employing the attenuated total reflection (ATR) technique. Ultraviolet-visible (UV-Vis) spectra were acquired using a Varian Cary-50 UV-Vis spectrophotometer (Varian, Inc., Palo Alto, CA, USA). X-ray photoelectron spectroscopy (XPS) was performed on an EXCALAB 250 XI X-ray photoelectron spectrometer (Thermo Scientific, Waltham, MA, USA). Energy-dispersive X-ray spectroscopy (EDS) was conducted using a ZEISS EVO 18 scanning electron microscope (ZEISS Group, Oberkochen, Germany). Transmission electron microscopy (TEM) images were obtained using a HITACHI HT7700 transmission electron microscope (Hitachi, Japan), and samples were prepared by dropping aqueous solutions onto copper grids. Dynamic light scattering (DLS) and zeta potential measurements were performed using an LA-950S2 laser particle size analyzer (Horiba, Kyoto, Japan). The high-performance liquid chromatography – mass spectrometry (HPLC-MS) was carried out on an Agilent 1260 Infinity II Bio-SEC system (Agilent Technologies, Inc., CA, USA). Inductively coupled plasma-mass spectrometry (ICP-MS) was performed with an iCAP PRO instrument (Thermo Scientific, Waltham, MA, USA). Cytotoxicity assays were performed on a TECAN M1000PRO microplate reader (Infinite M1000 Pro, TECAN, Switzerland) by measuring absorbance at 450 nm.

#### 3.2. Synthesis of $[\text{Ga}(\text{L})_2]\text{NO}_3$

$\text{Ga}(\text{NO}_3)_3 \cdot 9\text{H}_2\text{O}$  (2.5 mg, 6.0  $\mu\text{mol}$ ) and HL (3.0 mg, 7.3  $\mu\text{mol}$ ) were added into a 10 mL centrifuge tube, and MeOH (3 mL) was then added dropwise under ambient conditions to achieve complete dissolution. The reaction mixture was stirred at room temperature for 24 h, followed by centrifugation to remove the precipitate. The clear yellow solution was diffused with anhydrous ether to give yellow block crystals of  $[\text{Ga}(\text{L})_2]\text{NO}_3$  in the form of  $\text{CH}_3\text{OH}$  solvate after 7 days. The crystals were filtered, washed with anhydrous ether, and dried. Yield: 0.8 mg (23.3% based on HL). IR (ATR,  $\text{cm}^{-1}$ ): 3360(m), 2920(s), 2850(m), 1633(w), 1598(m), 1513(s), 1488(s), 1463(s), 1425(vs), 1362(vs), 1336(s), 1299(vs), 1276(vs), 1237(vs), 1224(vs), 1202(vs), 1173(s), 1133(vs), 1097(s), 1057(s), 1009(vs),

980(s), 956(m), 912(s), 870(w), 854(w), 823(s), 792(s), 746(s), 725(m), 696(w), 661(m), 646(m), 613(m).  $^1\text{H}$  NMR (400 MHz, DMSO-*d*<sub>6</sub>)  $\delta$  8.89 (d, *J* = 3.8 Hz, 2H), 8.32 (d, *J* = 7.7 Hz, 2H), 8.26 – 8.11 (m, 6H), 7.84 (d, *J* = 8.0 Hz, 2H), 7.76 – 7.66 (m, 4H), 7.18 (d, *J* = 3.2 Hz, 2H), 6.89 (d, *J* = 3.2 Hz, 2H), 3.94 (s, 8H), 3.49 (s, 8H).

### 3.3. Single-Crystal X-Ray Crystallography

Diffraction data were acquired on a Bruker APEX II CCD X-ray diffractometer (Bruker AXS GmbH, Germany) using Mo-K $\alpha$  ( $\lambda$  = 0.71073 Å) irradiation for  $[\text{Ga}(\text{L})_2]\text{NO}_3$ . Refinement and reduction of the collected data were achieved using the program SAINT, and absorption corrections were performed using a multi-scan method.[59] The crystal structures of  $[\text{Ga}(\text{L})_2]\text{NO}_3$  were solved by direct methods and refined on *F*<sup>2</sup> by full-matrix least-squares techniques with SHELXTL-2016 [60].

Crystallographic data for  $[\text{Ga}(\text{L})_2]\text{NO}_3$  have been deposited in the Cambridge Crystallographic Data Center (CCDC) as supplementary publication number 2482780. These data can be obtained free of charge either from the CCDC via [www.ccdc.cam.ac.uk/data\\_request/cif](http://www.ccdc.cam.ac.uk/data_request/cif) or from the Supplementary Information. A summary of the key crystallographic data for  $[\text{Ga}(\text{L})_2]\text{NO}_3$  is listed in Table 1.

### 3.4. $\text{Fe}^{2+}$ -Exchange with $[\text{Ga}(\text{L})_2]\text{NO}_3$

$[\text{Ga}(\text{L})_2]\text{NO}_3$  (3.0 mg, 3.2  $\mu\text{mol}$ ) and  $(\text{NH}_4)_2\text{Fe}(\text{SO}_4)_2\cdot 6\text{H}_2\text{O}$  (1.2 mg, 3.2  $\mu\text{mol}$ ) were dissolved in 5 mL of DMF, and the mixture was stirred at room temperature for 72 h. The solution color gradually changed from orange-yellow to dark green. A portion of 50 mL H<sub>2</sub>O was then introduced, and the solution was extracted three times with 80 mL CH<sub>2</sub>Cl<sub>2</sub>. The CH<sub>2</sub>Cl<sub>2</sub> layer was then combined, and the solvent was removed by rotary evaporation to give the yellowish-brown powder.

### 3.5. $\text{Fe}^{3+}$ -Exchange with $[\text{Ga}(\text{L})_2]\text{NO}_3$

$[\text{Ga}(\text{L})_2]\text{NO}_3$  (3.0 mg, 3.2  $\mu\text{mol}$ ) and  $\text{NH}_4\text{Fe}(\text{SO}_4)_2\cdot 12\text{H}_2\text{O}$  (1.5 mg, 3.2  $\mu\text{mol}$ ) were dissolved in 5 mL of DMF, and the mixture was stirred at room temperature for 72 h. The solution changed from orange-yellow to yellowish-brown. A portion of 50 mL H<sub>2</sub>O was then introduced, and the solution was extracted three times with 80 mL CH<sub>2</sub>Cl<sub>2</sub>. The CH<sub>2</sub>Cl<sub>2</sub> layer was then combined, and the solvent was removed by rotary evaporation to give the yellowish-brown powder.

### 3.6. Titration Experiment

For the titration with  $\text{Fe}^{2+}$ , a DMF solution of  $[\text{Ga}(\text{L})_2]\text{NO}_3$  with a concentration of  $1.06 \times 10^{-3}$  mol·L<sup>-1</sup> and an aqueous solution of  $(\text{NH}_4)_2\text{Fe}(\text{SO}_4)_2\cdot 6\text{H}_2\text{O}$  with a concentration of  $1.28 \times 10^{-2}$  mol·L<sup>-1</sup> were prepared as the titrant. Eight aliquots (3 mL each) of the complex solution were treated with different volumes of the  $\text{Fe}^{2+}$  titrant to achieve  $\text{Fe}^{2+}$  equivalent ratios of 0, 0.2, 0.4, 0.6, 0.8, 1.0, 1.2, and 1.4 eq relative to the complex. After reacting at room temperature for 0.5 h, 6 h, and 72 h, respectively, each reaction mixture was diluted 40 times with DMF, and its spectral changes were monitored by UV-Vis spectroscopy. The titration experiments with  $\text{Fe}^{3+}$  were carried out in the same manner using  $\text{NH}_4\text{Fe}(\text{SO}_4)_2\cdot 12\text{H}_2\text{O}$ .

### 3.7. Nanoparticle Formations of $[\text{Ga}(\text{L})_2]\text{A}$

$[\text{Ga}(\text{L})_2]\text{NO}_3$  (10.0 mg, 10.6  $\mu\text{mol}$ ) was dissolved in DMSO (1 mL) and then added dropwise to an aqueous solution of sodium hyaluronate (68.8 mg in 11 mL of water). The mixture was stirred at r.t. and protected from light for 72 h to obtain the resulting nanoparticles, which were dialyzed for 24 h (molecular weight cut-off of 1000 Da) to obtain  $[\text{Ga}(\text{L})_2]\text{A}$ .

### 3.8. *In Vitro* Cytotoxicity Evaluation by CCK-8 Assay

The NCI-H82 cell line (suspension-grown) was cultured in RPMI 1640 medium supplemented with 10% FBS, 1% P/S, or RPMI 1640 medium containing 1% P/S. Specifically, the suspension-grown

cells were centrifuged, and the supernatant was discarded. The cells were resuspended in serum-supplemented RPMI 1640 medium at a concentration of  $1 \times 10^5$  cells  $\text{mL}^{-1}$ . These cells were cultured at  $37^\circ\text{C}$  under a 5%  $\text{CO}_2$  atmosphere for the CCK-8 assays.

NCI-H82 cells were seeded at a density of  $2 \times 10^4$  cells per well in 100  $\mu\text{L}$  of serum-free medium (RPMI 1640 + 1% P/S) containing various concentrations of HL,  $[\text{Ga(L)}_2]\text{A}$ . All experiments were conducted with five replicates ( $n = 5$ ), using untreated cells as the 100% cell viability control and cell-free medium (RPMI 1640 + 10  $\mu\text{L}$  FBS + 1% P/S + CCK-8) as the blank.

The NCI-H82 cells were incubated continuously for 72 hours. After the incubation period, 10  $\mu\text{L}$  FBS and 10  $\mu\text{L}$  CCK-8 were added to the wells, and the plates were further incubated for 3.5 hours before analysis at 450 nm using a microplate reader. The relative cell viability (%) was calculated using equation (1) as described below:

$$V\% = \frac{[A]_{\text{experimental}} - [A]_{\text{blank}}}{[A]_{\text{control}} - [A]_{\text{blank}}} \times 100\% \quad (1)$$

in which  $V\%$  is the percentage of cell viability,  $[A]_{\text{experimental}}$  is the absorbance of the wells culturing the treated cells,  $[A]_{\text{blank}}$  is the absorbance of the blank, and  $[A]_{\text{control}}$  is the absorbance of the wells culturing untreated cells.

The A549 cell line (adherent cells) was cultured in Ham's F-12 medium supplemented with 10% FBS, 1% P/S, or Ham's F-12 medium containing 1% P/S. Specifically, the adherent cells grew as a monolayer and were detached at confluence using trypsin (0.5% w/v in PBS). After trypsinization, the cells were incubated for 3 minutes, centrifuged, and the supernatant was discarded. A 3 mL portion of serum-supplemented culture medium was added to neutralize any residual trypsin. The cells were re-suspended in serum-supplemented Ham's F-12 medium at a concentration of  $1 \times 10^5$  cells  $\text{mL}^{-1}$  and cultured under standard conditions ( $37^\circ\text{C}$ , 5%  $\text{CO}_2$ ) for the CCK-8 studies.

A549 cells were seeded at a density of  $1 \times 10^4$  cells per well in 90  $\mu\text{L}$  of culture medium (Ham's F-12 + 10% FBS + 1% P/S) and cultured for 24 hours at  $37^\circ\text{C}$  and 5%  $\text{CO}_2$  to allow cell attachment. The culture medium was then replaced with serum-free medium (Ham's F-12 + 1% P/S) containing various concentrations of the HL,  $[\text{Ga(L)}_2]\text{A}$ . All experiments were performed with five replicates ( $n = 5$ ), using untreated cells as the 100% cell viability control and cell-free medium (Ham's F-12 + 10% FBS + 1% P/S + CCK-8) as the blank.

The A549 cells were incubated continuously for 72 hours. After the incubation period, 10  $\mu\text{L}$  of FBS and 10  $\mu\text{L}$  of CCK-8 were added to each well, and the plates were incubated for an additional 2.5 h before being analyzed at 450 nm using a microplate reader. The relative cell viability (%) was calculated using Equation 1 above.

For the KYSE-510 (adherent cells) and Te-1 (adherent cells) cell lines, the cytotoxicity assessment followed a similar protocol to that of the A549 cells, with the exception of the culture media. KYSE-510 cells were cultured in a 1 : 1 mixture of RPMI 1640 and Ham's F-12 media, while Te-1 cells were cultured in RPMI 1640 medium. The exact compositions were: RPMI 1640 : Ham's F-12 = 1 : 1 + 10% FBS + 1% P/S and RPMI 1640 : Ham's F-12 = 1 : 1 + 1% P/S for KYSE-510; RPMI 1640 + 10% FBS + 1% P/S and RPMI 1640 + 1% P/S for Te-1.

### 3.9. Cellular Uptake

KYSE-510 cells were seeded into six 10 cm cell culture dishes at a density of  $2 \times 10^5$  cells per dish. Cells were cultured in serum-supplemented medium (RPMI 1640 : Ham's F-12 = 1:1 + 10% FBS + 1% P/S) until reaching approximately 95% confluence. The medium was then replaced with serum-free medium. To distinguish the group pretreated with sodium hyaluronate from the direct treatment group, designated  $[\text{Ga(L)}_2]\text{A}$ , the pretreated group was labeled  $[\text{Ga(L)}_2]\text{A}'$ . For the pretreated group, dishes were pretreated with 30 mg of sodium hyaluronate for 24 h prior to the addition of  $[\text{Ga(L)}_2]\text{A}$ , while the  $[\text{Ga(L)}_2]\text{A}$  group was administered with the drug directly. Both groups were exposed to  $[\text{Ga(L)}_2]\text{A}$  at a final HL concentration of 50  $\mu\text{M}$ . Cells were incubated with the compound for 2 h, 4 h, or 6 h. Following incubation, cells were washed three times with PBS buffer and harvested via trypsin

digestion. The harvested cells were collected into 15-mL centrifuge tubes and centrifuged at 900 rpm for 3 min. The resulting pellet was washed twice with PBS and centrifuged again. For metal content analysis, the cell pellet was digested with 0.4 mL concentrated nitric acid. The digest was diluted to 3 mL with deionized water, filtered through a 0.45  $\mu$ m membrane, and subjected to ICP-MS analysis to quantify the Ga<sup>3+</sup> concentration.

## 4. Conclusion

Intrigued by the nontoxicity and biocompatibility of Ga<sup>3+</sup> and the profound links between Ga<sup>3+</sup> and Fe<sup>3+</sup>, we herein demonstrate preliminarily that the thiosemicarbazone ligand HL can form a cationic octahedral complex of  $[\text{Ga}(\text{L})_2]\text{NO}_3$  with Ga<sup>3+</sup>. The nitrate-for-hyaluronate surrogation further yielded  $[\text{Ga}(\text{L})_2]\text{A}$  as a nanomedicine that endows the material with aqueous solubility and cell selectivity. The facile yet gradual metathesis of  $[\text{Ga}(\text{L})_2]\text{NO}_3$  with both Fe<sup>2+</sup> and Fe<sup>3+</sup> indicated that  $[\text{Ga}(\text{L})_2]\text{NO}_3$  can be a promising anticancer drug with 'stealth' properties during drug delivery. Nevertheless, substantial future work regarding the mechanisms of action, oral bioavailability, and in vivo performance is needed in the future.

**Supplementary Materials:** The following supporting information can be downloaded at: Preprints.org, Additional structure diagrams, spectroscopies, and spectrometry.

**Author Contributions:** Conceptualization, W.H.Z.; methodology, Y.N.; validation, M.L.D. and W.H.Z.; formal analysis, Y.N.; data curation, Y.N.; writing—original draft preparation, Y.N.; writing—review and editing, W.H.Z. and D.J.Y.; supervision, W.H.Z.; project administration, W.H.Z.; funding acquisition, W.H.Z. All authors have read and agreed to the published version of the manuscript.

**Funding:** This work was financially supported by Suzhou Municipal Health Commission (MSXM2024020, SKYD2023143), Suzhou Municipal Science and Technology Bureau (SKY2023203), and Guangdong Provincial Key Laboratory of New Drug Screening, Southern Medical University.

**Conflicts of Interest:** The authors declare no conflict of interest.

## References

1. Kalinowski, D.S.; Quach, P.; Richardson, D.R. Thiosemicarbazones: The new wave in cancer treatment. *Future Med. Chem.* **2009**, *1*, 1143–1151.
2. Serda, M.; Kalinowski, D.S.; Rasko, N.; Potůčková, E.; Mrozek-Wilczkiewicz, A.; Musiol, R.; Małecki, J.G.; Sajewicz, M.; Ratuszna, A.; Muchowicz, A., *et al.* Exploring the anti-cancer activity of novel thiosemicarbazones generated through the combination of retro-fragments: Dissection of critical structure-activity relationships. *PLOS One* **2014**, *9*, e110291.
3. Dilworth, J.R.; Huetting, R. Metal complexes of thiosemicarbazones for imaging and therapy. *Inorg. Chim. Acta* **2012**, *389*, 3–15.
4. Shakya, B.; Yadav, N.P. Thiosemicarbazones as potent anticancer agents and their modes of action. *Mini. Rev. Med. Chem.* **2020**, *20*, 638–661.
5. Rudnev, A.V.; Foteva, L.S.; Kowol, C.; Berger, R.; Jakupc, M.A.; Arion, V.B.; Timerbaev, A.R.; Keppler, B.K. Preclinical characterization of anticancer gallium(III) complexes: Solubility, stability, lipophilicity and binding to serum proteins. *J. Inorg. Biochem.* **2006**, *100*, 1819–1826.
6. Kowol, C.R.; Berger, R.; Eichinger, R.; Roller, A.; Jakupc, M.A.; Schmidt, P.P.; Arion, V.B.; Keppler, B.K. Gallium(III) and iron(III) complexes of  $\alpha$ -N-heterocyclic thiosemicarbazones: Synthesis, characterization, cytotoxicity, and interaction with ribonucleotide reductase. *J. Med. Chem.* **2007**, *50*, 1254–1265.
7. Yuan, J.; Lovejoy, D.B.; Richardson, D.R. Novel di-2-pyridyl-derived iron chelators with marked and selective antitumor activity: In vitro and in vivo assessment. *Blood* **2004**, *104*, 1450–1458.
8. Richardson, D.R.; Kalinowski, D.S.; Richardson, V.; Sharpe, P.C.; Lovejoy, D.B.; Islam, M.; Bernhardt, P.V. 2-acetylpyridine thiosemicarbazones are potent iron chelators and antiproliferative agents: Redox activity, iron complexation and characterization of their antitumor activity. *J. Med. Chem.* **2009**, *52*, 1459–1470.

9. Lovejoy, D.B.; Sharp, D.M.; Seebacher, N.; Obeidy, P.; Prichard, T.; Stefani, C.; Basha, M.T.; Sharpe, P.C.; Jansson, P.J.; Kalinowski, D.S., *et al.* Novel second-generation di-2-pyridylketone thiosemicarbazones show synergism with standard chemotherapeutics and demonstrate potent activity against lung cancer xenografts after oral and intravenous administration in vivo. *J. Med. Chem.* **2012**, *55*, 7230–7244.
10. Ma, B.; Goh, B.C.; Tan, E.H.; Lam, K.C.; Soo, R.; Leong, S.S.; Wang, L.Z.; Mo, F.; Chan, A.T.C.; Zee, B., *et al.* A multicenter phase II trial of 3-aminopyridine-2-carboxaldehyde thiosemicarbazone (3-AP, Triapine®) and gemcitabine in advanced non-small-cell lung cancer with pharmacokinetic evaluation using peripheral blood mononuclear cells. *Invest. New Drugs* **2008**, *26*, 169–173.
11. DeConti, R.C.; Toftness, B.R.; Agrawal, K.C.; Tomchick, R.; Mead, J.A.R.; Bertino, J.R.; Sartorelli, A.C.; Creasey, W.A. Clinical and pharmacological studies with 5-hydroxy-2-formylpyridine thiosemicarbazone. *Cancer Res.* **1972**, *32*, 1455–1462.
12. Westin, S.N.; Nieves-Neira, W.; Lynam, C.; Salim, K.Y.; Silva, A.D.; Ho, R.T.; Mills, G.B.; Coleman, R.L.; Janku, F.; Matei, D. Abstract CT033: Safety and early efficacy signals for COTI-2, an orally available small molecule targeting p53, in a phase I trial of recurrent gynecologic cancer. *Cancer Res.* **2018**, *78*, CT033–CT033.
13. Bormio Nunes, J.H.; Hager, S.; Mathuber, M.; Pósa, V.; Roller, A.; Enyedy, É.A.; Stefanelli, A.; Berger, W.; Keppler, B.K.; Heffeter, P., *et al.* Cancer cell resistance against the clinically investigated thiosemicarbazone COTI-2 is based on formation of intracellular copper complex glutathione adducts and ABCC1-mediated efflux. *J. Med. Chem.* **2020**, *63*, 13719–13732.
14. Lessa, J.A.; Parrilha, G.L.; Beraldo, H. Gallium complexes as new promising metallodrug candidates. *Inorg. Chim. Acta* **2012**, *393*, 53–63.
15. Bernstein, L.R. Mechanisms of therapeutic activity for Gallium. *Pharmacol. Rev.* **1998**, *50*, 665–682.
16. Zhang, X.; Yang, X.-R.; Huang, X.-W.; Wang, W.-M.; Shi, R.-Y.; Xu, Y.; Wang, Z.; Qiu, S.-J.; Fan, J.; Zhou, J. Sorafenib in treatment of patients with advanced hepatocellular carcinoma: A systematic review. *Hepatob. Pancreat. Dis.* **2012**, *11*, 458–466.
17. Collery, P.; Keppler, B.; Madoulet, C.; Desoize, B. Gallium in cancer treatment. *Crit. Rev. Oncol. Hemat.* **2002**, *42*, 283–296.
18. He, J.; Ye, Y.; Zhang, D.; Yao, K.; Zhou, M. Visualized Gallium/lyticase-integrated antifungal strategy for fungal keratitis treatment. *Adv. Mater.* **2022**, *34*, 2206437.
19. Hofheinz, R.; Dittrich, C.; Jakupc, M.A.; Drescher, A.; Jaehde, U.; Gneist, M.; Graf von Keyserlingk, N.; Keppler, B.K.; Hochhaus, A. Early results from a phase I study on orally administered tris(8-quinolinolato)gallium(III) (FFC11, KP46) in patients with solid tumors--a CESAR study (Central European Society for Anticancer Drug Research--EWIV). *Int. J. Clin. Pharm. Th.* **2005**, *43*, 590–591.
20. Wilke, N.L.; Abodo, L.O.; Frias, C.; Frias, J.; Baas, J.; Jakupc, M.A.; Keppler, B.K.; Prokop, A. The gallium complex KP46 sensitizes resistant leukemia cells and overcomes Bcl-2-induced multidrug resistance in lymphoma cells via upregulation of Harakiri and downregulation of XIAP in vitro. *Biomed. Pharmacother.* **2022**, *156*, 113974.
21. Hreusova, M.; Novohradsky, V.; Markova, L.; Kostrhunova, H.; Potočnák, I.; Brabec, V.; Kasparkova, J. Gallium(III) complex with cloxyquin ligands induces ferroptosis in cancer cells and is a potent agent against both differentiated and tumorigenic cancer stem rhabdomyosarcoma cells. *Bioinorg. Chem. Appl.* **2022**, *2022*, 3095749.
22. Luo, S.-Y.; Zeng, C.-M.; Xu, P.; Ning, Y.; Dong, M.-L.; Zhang, W.-H.; Yu, G. Thiazole functionalization of thiosemicarbazone for Cu(II) complexation: Moving toward highly efficient anticancer drugs with promising oral bioavailability. *Molecules* **2024**, *29*, 3832.
23. Cao, F.-L.; Zhang, Z.-S.; Dong, M.-L.; Ning, Y.; Zhang, W.-H.; Mao, Y.; Young, D.J. A high-entropy coordination cage featuring an Au-porphyrin metalloligand for the photodynamic therapy of liver cancer. *Chem. Commun.* **2025**, *61*, 6663–6666.
24. Li, W.; Li, R.; Ye, Q.; Zou, Y.; Lu, X.; Zhang, W.; Chen, J.; Zhao, Y. Mn<sub>3</sub>O<sub>4</sub> nanoshell coated metal-organic frameworks with microenvironment-driven O<sub>2</sub> production and GSH exhaustion ability for enhanced chemodynamic and photodynamic cancer therapies. *Adv. Healthc. Mater.* **2023**, *12*, 2202280.

25. Hou, Y.-K.; Zhang, Z.-J.; Li, R.-T.; Peng, J.; Chen, S.-Y.; Yue, Y.-R.; Zhang, W.-H.; Sun, B.; Chen, J.-X.; Zhou, Q. Remodeling the tumor microenvironment with core–shell nanosensitizer featuring dual-modal imaging and multimodal therapy for breast cancer. *ACS Appl. Mater. Interfaces* **2023**, *15*, 2602–2616.

26. Stefani, C.; Punnia-Moorthy, G.; Lovejoy, D.B.; Jansson, P.J.; Kalinowski, D.S.; Sharpe, P.C.; Bernhardt, P.V.; Richardson, D.R. Halogenated 2'-benzoylpyridine thiosemicarbazone (XBpT) chelators with potent and selective anti-neoplastic activity: Relationship to intracellular redox activity. *J. Med. Chem.* **2011**, *54*, 6936–6948.

27. Kalinowski, D.S.; Yu, Sharpe, P.C.; Islam, M.; Liao, Y.-T.; Lovejoy, D.B.; Kumar, N.; Bernhardt, P.V.; Richardson, D.R. Design, synthesis, and characterization of novel iron chelators: Structure–activity relationships of the 2-benzoylpyridine thiosemicarbazone series and their 3-nitrobenzoyl analogues as potent antitumor agents. *J. Med. Chem.* **2007**, *50*, 3716–3729.

28. Milunovic, M.N.M.; Ohui, K.; Besleaga, I.; Petrasheuskaya, T.V.; Dömöötör, O.; Enyedy, É.A.; Darvasiova, D.; Rapti, P.; Barbieriková, Z.; Vegh, D., *et al.* Copper(II) complexes with isomeric morpholine-substituted 2-formylpyridine thiosemicarbazone hybrids as potential anticancer drugs inhibiting both ribonucleotide reductase and tubulin polymerization: The morpholine position matters. *J. Med. Chem.* **2024**, *67*, 9069–9090.

29. Man, X.; Li, S.; Xu, G.; Li, W.; Zhu, M.; Zhang, Z.; Liang, H.; Yang, F. Developing a copper(II) isopropyl 2-pyridyl ketone thiosemicarbazone compound based on the IB subdomain of human serum albumin-indomethacin complex: Inhibiting tumor growth by remodeling the tumor microenvironment. *J. Med. Chem.* **2024**, *67*, 5744–5757.

30. Li, A.; Huang, K.; Pan, W.; Wu, Y.; Liang, Y.; Zhang, Z.; Wu, D.; Ma, L.; Gou, Y. Thiosemicarbazone mixed-valence Cu(I/II) complex against lung adenocarcinoma cells through multiple pathways involving cuproptosis. *J. Med. Chem.* **2024**, *67*, 9091–9103.

31. Stacy, A.E.; Palanimuthu, D.; Bernhardt, P.V.; Kalinowski, D.S.; Jansson, P.J.; Richardson, D.R. Zinc(II)-thiosemicarbazone complexes are localized to the lysosomal compartment where they transmetallate with copper ions to induce cytotoxicity. *J. Med. Chem.* **2016**, *59*, 4965–4984.

32. Qi, J.; Zhao, W.; Zheng, Y.; Wang, R.; Chen, Q.; Wang, F.-A.; Fan, W.; Gao, H.; Xia, X. Single-crystal structure and intracellular localization of Zn(II)-thiosemicarbazone complex targeting mitochondrial apoptosis pathways. *Bioorg. Med. Chem. Lett.* **2020**, *30*, 127340.

33. Carcelli, M.; Tegoni, M.; Bartoli, J.; Marzano, C.; Pelosi, G.; Salvalaio, M.; Rogolino, D.; Gandin, V. In vitro and in vivo anticancer activity of tridentate thiosemicarbazone copper complexes: Unravelling an unexplored pharmacological target. *Eur. J. Med. Chem.* **2020**, *194*, 112266.

34. Kaya, B.; Gholam Azad, M.; Suleymanoglu, M.; Harmer, J.R.; Wijesinghe, T.P.; Richardson, V.; Zhao, X.; Bernhardt, P.V.; Dharmasivam, M.; Richardson, D.R. Isosteric replacement of sulfur to selenium in a thiosemicarbazone: Promotion of Zn(II) complex dissociation and transmetalation to augment anticancer efficacy. *J. Med. Chem.* **2024**, *67*, 12155–12183.

35. Fathy, A.; Ibrahim, A.B.M.; Elkhalik, S.A.; Villinger, A.; Abbas, S.M. New iron(III) complexes with 2-formylpyridine thiosemicarbazones: Synthetic aspects, structural and spectral analyses and cytotoxicity screening against MCF-7 human cancer cells. *Helijon* **2023**, *9*, e13008.

36. Wiles, D.M.; Suprunchuk, T. The C=S stretching vibration in the infrared spectra of some thiosemicarbazones. II. Aldehyde thiosemicarbazones containing aromatic groups. *Can. J. Chem.* **1967**, *45*, 2258–2263.

37. West, D.X.; Billeh, I.S.; Jasinski, J.P.; Jasinski, J.M.; Butcher, R.J. Complexes of N(4)-cyclohexylsemicarbazones and N(4)-cyclohexylthiosemicarbazones derived from 2-formyl-, 2-acetyl- and 2-benzoylpyridine. *Transition Met. Chem.* **1998**, *23*, 209–214.

38. Quiroga, A.G.; M. Pérez, J.; López-Solera, I.; Montero, E.I.; Masaguer, J.R.; Alonso, C.; Navarro-Ranninger, C. Binuclear chloro-bridged palladated and platinated complexes derived from *p*-isopropylbenzaldehyde thiosemicarbazone with cytotoxicity against cisplatin resistant tumor cell lines. *J. Inorg. Biochem.* **1998**, *69*, 275–281.

39. John, R.P.; Sreekanth, A.; Rajakannan, V.; Ajith, T.A.; Kurup, M.R.P. New copper(II) complexes of 2-hydroxyacetophenone N(4)-substituted thiosemicarbazones and polypyridyl co-ligands: Structural, electrochemical and antimicrobial studies. *Polyhedron* **2004**, *23*, 2549–2559.

40. Wu, K.-Y.; Qin, L.; Fan, C.; Cai, S.-L.; Zhang, T.-T.; Chen, W.-H.; Tang, X.-Y.; Chen, J.-X. Sequential and recyclable sensing of  $\text{Fe}^{3+}$  and ascorbic acid in water with a terbium(III)-based metal-organic framework. *Dalton Trans.* **2019**, *48*, 8911–8919.

41. Bourque, J.L.; Biesinger, M.C.; Baines, K.M. Chemical state determination of molecular gallium compounds using XPS. *Dalton Trans.* **2016**, *45*, 7678–7696.

42. Hao, H.; Chen, X.; Li, Z.; Shen, Y.; Wang, H.; Zhao, Y.; Huang, R.; Liu, T.; Liang, J.; An, Y., *et al.* Remote plasma-enhanced atomic layer deposition of gallium oxide thin films with  $\text{NH}_3$  plasma pretreatment. *J. Semicond.* **2019**, *40*, 012806.

43. Zatsepin, D.A.; Boukhvalov, D.W.; Zatsepin, A.F. Quality assessment of GaN epitaxial films: Acidification scenarios based on XPS-and-DFT combined study. *Appl. Surf. Sci.* **2021**, *563*, 150308.

44. Borges, R.H.U.; Paniago, E.; Bernaldo, H. Equilibrium and kinetic studies of iron(II) and iron(III) complexes of some  $\alpha$ (N)-heterocyclic thiosemicarbazones. Reduction of the iron(III) complexes of 2-formylpyridine thiosemicarbazone and 2-acetylpyridine thiosemicarbazone by cellular thiol-like reducing agents. *J. Inorg. Biochem.* **1997**, *65*, 267–275.

45. Alcaraz, R.; Muñiz, P.; Cavia, M.; Palacios, Ó.; Samper, K.G.; Gil-García, R.; Jiménez-Pérez, A.; García-Tojal, J.; García-Girón, C. Thiosemicarbazone-metal complexes exhibiting cytotoxicity in colon cancer cell lines through oxidative stress. *J. Inorg. Biochem.* **2020**, *206*, 110993.

46. Liu, H.; Feng, X.-D.; Yang, B.; Tong, R.-L.; Lu, Y.-J.; Chen, D.-Y.; Zhou, L.; Xie, H.-Y.; Zheng, S.-S.; Wu, J. Dimethyl fumarate suppresses hepatocellular carcinoma progression via activating SOCS3/JAK1/STAT3 signaling pathway. *Am. J. Transl. Res.* **2019**, *11*, 4713–4725.

47. Li, H.; Wang, Y.; Su, R.; Jia, Y.; Lai, X.; Su, H.; Fan, Y.; Wang, Y.; Xing, W.; Qin, J. Dimethyl fumarate combined with vemurafenib enhances anti-melanoma efficacy via inhibiting the Hippo/YAP, NRF2-ARE, and AKT/mTOR/ERK pathways in A375 melanoma cells. *Front. Oncol.* **2022**, *12*, 794216.

48. Basilotta, R.; Lanza, M.; Filippone, A.; Casili, G.; Mannino, D.; De Gaetano, F.; Chisari, G.; Colarossi, L.; Motta, G.; Campolo, M., *et al.* Therapeutic potential of dimethyl fumarate in counteract oral squamous cell carcinoma progression by modulating apoptosis, oxidative stress and epithelial–mesenchymal transition. *Int. J. Mol. Sci.* **2023**, *24*, 2777.

49. Huang, N.; Tang, X.-Y.; Meng, W.; Lai, Y.-H.; Zhou, X.; Yu, X.-Z.; Zhang, W.-H.; Chen, J.-X. Immunogenic radiation therapy for enhanced antitumor immunity via a core–shell nanosensitizer-mediated immunosuppressive tumor microenvironment modulation. *ACS Nano* **2023**, *17*, 19853–19864.

50. Öztürk, K.; Kaplan, M.; Çalış, S. Effects of nanoparticle size, shape, and zeta potential on drug delivery. *Int. J. Pharm.* **2024**, *666*, 124799.

51. Maeda, H.; Nakamura, H.; Fang, J. The EPR effect for macromolecular drug delivery to solid tumors: improvement of tumor uptake, lowering of systemic toxicity, and distinct tumor imaging in vivo. *Adv. Drug Deliv. Rev.* **2013**, *65*, 71–79.

52. Zhang, L.; Liu, Y.; Liu, G.; Xu, D.; Liang, S.; Zhu, X.; Lu, Y.; Wang, H. Prolonging the plasma circulation of proteins by nano-encapsulation with phosphorylcholine-based polymer. *Nano Res.* **2016**, *9*, 2424–2432.

53. Mendes, I.C.; Soares, M.A.; dos Santos, R.G.; Pinheiro, C.; Bernaldo, H. Gallium(III) complexes of 2-pyridineformamide thiosemicarbazones: Cytotoxic activity against malignant glioblastoma. *Eur. J. Med. Chem.* **2009**, *44*, 1870–1877.

54. Kumar, K.; Schniper, S.; González-Sarriás, A.; Holder, A.A.; Sanders, N.; Sullivan, D.; Jarrett, W.L.; Davis, K.; Bai, F.; Seeram, N.P., *et al.* Highly potent anti-proliferative effects of a gallium(III) complex with 7-chloroquinoline thiosemicarbazone as a ligand: Synthesis, cytotoxic and antimalarial evaluation. *Eur. J. Med. Chem.* **2014**, *86*, 81–86.

55. Yang, T.; Zhang, Z.; Zhang, J.; Li, Y.; Li, W.; Liang, H.; Yang, F. Developing a Gallium(III) agent based on the properties of the tumor microenvironment and lactoferrin: Achieving two-agent co-delivery and multi-targeted combination therapy of cancer. *J. Med. Chem.* **2023**, *66*, 793–803.

56. Dharmasivam, M.; Kaya, B.; Wijesinghe, T.; Gholam Azad, M.; González, M.A.; Hussaini, M.; Chekmarev, J.; Bernhardt, P.V.; Richardson, D.R. Designing tailored thiosemicarbazones with bespoke properties: The styrene moiety imparts potent activity, inhibits heme center oxidation, and results in a novel “stealth Zinc(II) complex”. *J. Med. Chem.* **2023**, *66*, 1426–1453.

57. Bernhardt, P.V.; Sharpe, P.C.; Islam, M.; Lovejoy, D.B.; Kalinowski, D.S.; Richardson, D.R. Iron chelators of the dipyridylketone thiosemicarbazone class: Precomplexation and transmetalation effects on anticancer activity. *J. Med. Chem.* **2009**, *52*, 407–415.
58. Zhao, X.; Qian, Y.; Hu, S.; Tian, Y. Synthesis, anticancer activity and mechanism of action of Fe(III) complexes. *Drug Dev. Res.* **2024**, *85*, e22264.
59. Sheldrick, G.M. SADABS (Version 2.03): Program for empirical absorption correction of area detector data; University of Göttingen, Germany. **1996**.
60. Sheldrick, G.M. Crystal structure refinement with SHELXL. *Acta Crystallogr., Sect. C* **2015**, *71*, 3–8.

**Disclaimer/Publisher's Note:** The statements, opinions and data contained in all publications are solely those of the individual author(s) and contributor(s) and not of MDPI and/or the editor(s). MDPI and/or the editor(s) disclaim responsibility for any injury to people or property resulting from any ideas, methods, instructions or products referred to in the content.